JACS
JOURNAL OF THE AMERICAN CHEMICAL SOCIETY
Article
pubs.acs.org/JACS

The Ferraquinone–Ferrahydroquinone Couple: Combining Quinonic and Metal-Based Reactivity

Alexander Dauth,[†,§] Urs Gellrich,[†,§] Yael Diskin-Posner,[‡] Yehoshoa Ben-David,[†] and David Milstein*[,†]

[†]Department of Organic Chemistry and [‡]Department of Chemical Research Support, Weizmann Institute of Science, Rehovot 76100, Israel

Supporting Information

ABSTRACT: A ferraquinone–ferrahydroquinone organometallic redox couple was prepared and characterized. Intricate cooperativity of the metal was observed with different positions on the ligand. This allowed cooperative activation of small molecules like molecular hydrogen, oxygen, and bromine. Likewise, dehydrogenation of alcohols was achieved through 1,6 metal–ligand cooperation.

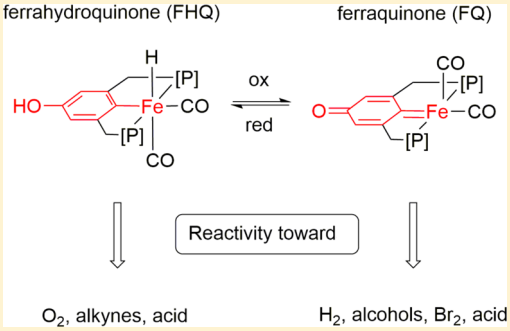

INTRODUCTION

Quinones are prevalent in biological and chemical redox processes.[1] For example, the production of hydrogen peroxide utilizing anthraquinone is performed yearly on a multiton scale.[2] Quinones like DDQ and chloranil are routinely used for oxidation reactions in academic laboratories.[3−9] Likewise, quinonic cofactors such as ubiquinone (coenzyme Q10) play an essential role in the respiratory chain of almost all aerobic organisms and act as antioxidants in the body.[10,11] Recently, quinones have also found utilization in transdisciplinary applications such as enzymatic fuel cells.[12] We sought to combine the redox properties of quinonic compounds with suitable transition metals in the anticipation of observing new cooperative patterns that can in turn lead to novel chemical transformations. To this end, we envisaged the employment of iron, which has experienced a renaissance in its use in transition metal catalysis due to its obvious ecological and economic benefits.[13−25]

Several years ago, our group reported the formation of the first and only metallaquinone, in which an oxygen atom of a quinone is replaced by a metal, namely, the ruthenaquinone depicted in Scheme 1.[26] Spectroscopic and computational studies of this new compound class were performed, but no further reactivity studies were undertaken. Specifically, the spectral properties were solvent-dependent, which was ascribed to the presence of an overall quinonic structure in nonpolar solvents whereas a zwitterionic structure was stabilized in more polar solvents.

Scheme 1. The Only Metallaquinone Reported to Date

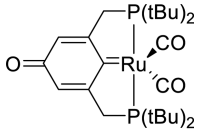

Ruthenaquinone

Other reports from our group described phenoxonium cations as well as quinone methides stabilized by transition metals.[27−29] A number of organometallic species are known that contain *o*- and *p*-quinonic moieties[30−32] in their ligand framework, but in no other case is the metal center an integral part of the quinonic system.[33−35] On the basis of our earlier findings,[26] we intended to prepare a corresponding complex of earth-abundant iron, ferraquinone **1**, with its hydrogenated counterpart, the ferrahydroquinone **2**, and to investigate the general reactivity of the resulting redox couple toward the activation of small molecules (Scheme 2).

Specifically, the role and mode of metal–ligand cooperation in this system was explored in the various transformations facilitated by the system. In recent years, cooperation between the metal and the supporting ligands has led to unprecedented

Scheme 2. The Envisioned Ferraquinone–Hydroferraquinone Redox Couple

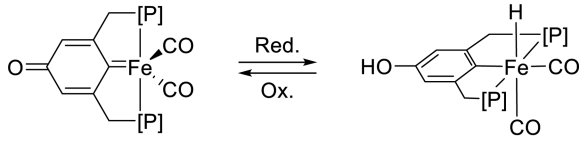

1 **2**

Received: December 20, 2016
Published: January 31, 2017

DOI: 10.1021/jacs.6b13050
J. Am. Chem. Soc. 2017, 139, 2799−2807

reactivity that harvests the reactivities of both the metal and the ligand.[36−40]

RESULTS AND DISCUSSION

The phenolic PCP pincer ligand 3,5-bis-(diisopropylphosphinomethylene)phenol (**3**) was prepared (see the Supporting Information) and reacted with $Fe(CO)_5$ in tetrahydrofuran (THF) under UVB irradiation (Scheme 3).

Scheme 3. Preparation of 1 and 2

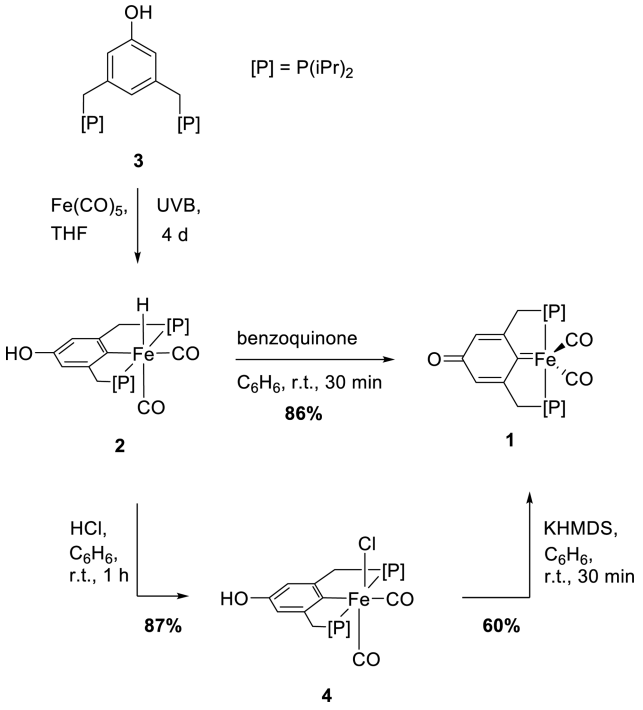

After 4 days, ligand metalation was complete, and a highly air-sensitive green crystalline solid was obtained. The product was identified by NMR analysis as ferrahydroquinone hydride **2**, exhibiting a clear triplet in the ^{1}H NMR spectrum at −8.83 ppm in C_6D_6 characteristic of a hydride cis to two equivalent P ligands and trans to CO as a strong π-acceptor ligand. The ring proton of the pincer ligand was found at 6.48 ppm, which is typical for the aromatic protons in organic hydroquinones.

X-ray-quality crystals were obtained by slow diffusion of pentane into an ether/pentane solution of **2** (Figure 1).[41] The unusually expansive unit cell (see the Supporting Information) contains 12 molecules in the asymmetric unit cell of **2** and confirms the formation of the ferrahydroquinone hydride dicarbonyl complex as a distorted octahedron. The bond distance between the iron center and the ipso carbon of the ligand (C1) is 2.070(4) Å. This is slightly longer than the Fe−C(ipso) distance in the related POCOP iron pincer dicarbonyl hydride complex reported by Guan and co-workers (1.995 Å).[42] In the ligand scaffold, the length of the C5−O1 bond is 1.440(6) Å, making it slightly longer than the C−O single bond in organic hydroquinone (1.392 Å). The P1−Fe−P2 and C1−Fe−C21 bond angles are smaller than 180° (159.10(6)° and 170.8(3)°, respectively), while the angle between the CO ligands is almost a proper right angle (88.8(3)°).

Ferrahydroquinone hydride **2** was treated with 2 equiv of benzoquinone in order to transform it to ferraquinone **1**. High-resolution mass spectrometry confirmed the formal loss of H_2

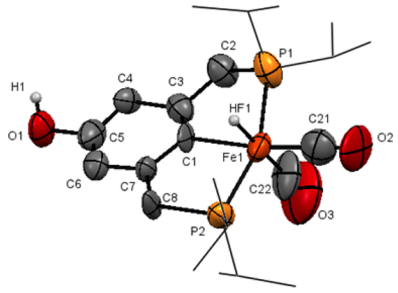

Figure 1. Solid-state structure of **2** (thermal ellipsoids set at the 50% probability level; isopropyl groups presented as wireframe and hydrogens omitted for clarity). Selected bond lengths [Å] and angles [deg] for **2**: Fe1−C21 1.747(8), Fe1−C22 1.640(6), Fe1−P1 2.239(2), Fe1−P2 2.276(2), Fe1−C1 2.070(4), C5−O1 1.440(6), C1−C7 1.394(6), C7−C6 1.427(6), C6−C5 1.340(7), P1−Fe1−P2 159.10(6), C1−Fe1−C21 170.8(3), C1−Fe1−C22 99.5(3), C21−Fe1−C22 88.8(3). Data collected at ESRF ID-29.[43]

by the dehydrogenation of **2** with benzoquinone. Further support for the formation of a quinonic structure comes from the NMR data, which show the signal of the ring proton in the phenyl moiety of the pincer ligand at 6.87 ppm, which is also typical for organic quinones. Likewise, the carbonyl carbon gives a signal at 170 ppm in the ^{13}C NMR spectrum, which is slightly upfield from those of organic quinones. The carbenoid ipso carbon could not be detected, possibly because of fast relaxation through the neighboring Fe center or the presence of trace paramagnetic impurities.[44] As X-ray-quality crystals could not be obtained, ferraquinone **1** was also prepared independently via a two-step sequence in order to confirm its formation (Scheme 3). In the first step, a benzene solution of **2** was treated with aqueous hydrochloric acid. The corresponding ferrahydroquinone chloride complex **4** was formed as a light-yellow solid in 87% yield. The ^{1}H NMR spectrum of **4** confirmed the elimination of the hydride ligand, and the solid-state structure also showed the replacement of the hydride by a chloride ligand (Figure 2).

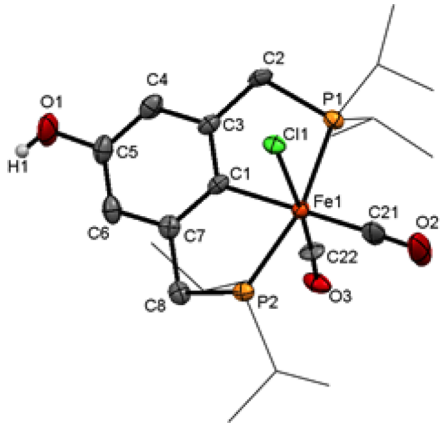

Figure 2. Solid-state structure of **4** (thermal ellipsoids set at the 50% probability level; isopropyl groups presented as wireframe and hydrogens omitted for clarity). Selected bond lengths [Å] and angles [deg] for **4**: Fe1−C21 1.801(5), Fe1−C22 1.66(1), Fe1−Cl1 2.402(4), Fe1−C1 2.041(4), Fe1−P1 2.265(2), Fe1−P2 2.274(2), C5−O1 1.381(6), C1−C7 1.402(8), C6−C7 1.400(7), C5−C6 1.384(8), P1−Fe1−P2 165.14(5), C1−Fe1−C21 179.6(4), C1−Fe1−Cl1 87.5(2), C21−Fe1−C22 93.6(4).

DOI: 10.1021/jacs.6b13050
J. Am. Chem. Soc. 2017, 139, 2799−2807

Again, the complex adopts a slightly distorted octahedral geometry, with an Fe1−C1 bond length of 2.041(4) Å and an Fe1−Cl1 distance of 2.402(4) Å. The ligand is aromatic, with C−C bond lengths varying slightly between 1.384 and 1.403 Å and the C−O bond being a typical hydroquinonic single bond at 1.381(6) Å. Consequently, the phenolic position of complex **4** was deprotonated with KHMDS in benzene, which led to the formation of ferraquinone **1** in 60% yield with identical spectral properties as observed after the reaction of **2** with benzoquinone. In contrast to the previously reported ruthenaquinone,[26] the spectral properties of **1** were not dependent on the polarity of the solvent, and it was found to be soluble in a wide spectrum of organic solvents ranging from methanol, acetonitrile, tetrahydrofuran, and dichloromethane to diethyl ether and pentane. The addition of external ligands such as CO, acetonitrile, or PPh_3 did not affect the spectral properties of **1**, signifying a coordinatively saturated complex. Indeed, density functional theory (DFT) calculations at the BP86-D3/def2-TZVP level clearly minimize **1** in a quinonic geometry as a trigonal bipyramid.[45] The C−O bond in the ligand was calculated to be a double bond at 1.25 Å, and the C−C bond lengths in the aryl moiety varied from 1.46 Å for the single bonds to 1.37 Å for the double bonds in conjugation with the quinonic C═O double bond (Figure 3). The angle

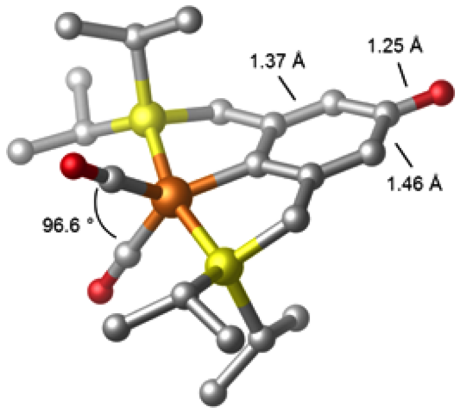

Figure 3. DFT-optimized structure of **1** (BP86-D3/def2-TZVP).

between the CO ligands is 96°, which is corroborated by the FT-IR spectrum of **1**, where the CO ligands appear as two bands of almost equal intensity at 1978 and 1919 cm^{-1}. These values are in turn in good agreement with the data reported for the ruthenaquinone system (1983 and 1926 cm^{-1}). The quinonic C═O bond stretch falls at a relatively low wavenumber (1563 cm^{-1}), suggesting a strong contribution of the metal center to the electronic structure of the ligand. This observation is qualitatively confirmed by frequency calculations at the BP86-D3/def2-TZVP level, rendering this band at 1583 cm^{-1}.

Having established synthetic routes to both members of the ferraquinone−ferrahydroquinone couple **1** and **2**, respectively, we set out to investigate their reactivity with special attention to cooperativity between the metal and the ligand.

Initially, we were interested in whether **1** could be directly transformed into **2** by activation of molecular hydrogen. When a solution of **1** in C_6D_6 was pressurized with 2 bar H_2, formation of **2** was observed after 18 h (Scheme 4). Under UVB irradiation, the reaction was complete after only 2 h.

Scheme 4. Reaction of 1 with H_2 via Formal 1,6-Addition

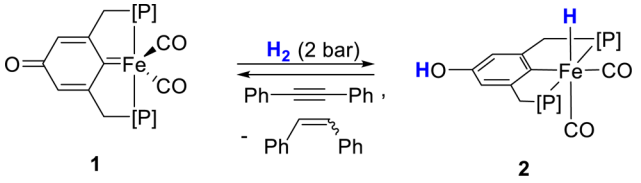

The mechanism of thermal hydrogen activation by ferraquinone **1** was examined by DFT calculations at the SMD(benzene)-TPSS-D3BJ/def2-TZVPP//BP86-D3/def2-SV(P) level of theory (Figure 4). Direct addition of H_2 to the

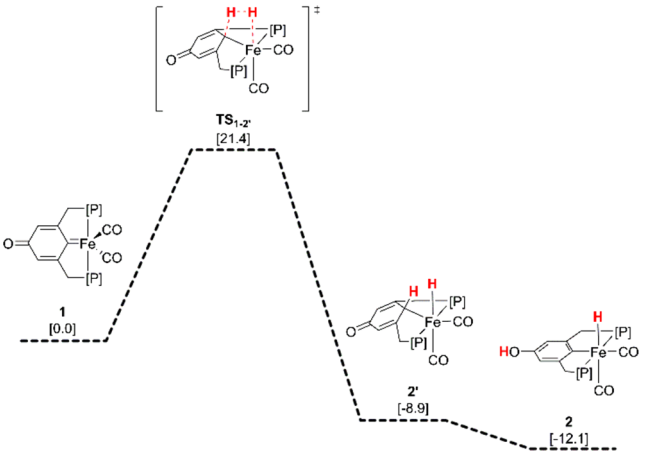

Figure 4. Free energy pathway for H_2 activation by ferraquinone **1** calculated at the TPSS-D3BJ/def2-TZVPP//BP86-D3/def2-SV(P) level of theory. Solvent effects were implicitly taken into account using the SMD model.

$Fe-C_{ipso}$ bond is possible according to the calculations via a low barrier of 21.4 kcal/mol. Subsequent keto−enol tautomerization yields ferrahydroquinone hydride **2** in an overall exergonic reaction.

The net reaction comprises a formal 1,6-type cooperation of the Fe center with the carbonyl oxygen at the para position of the ligand. Ferrahydroquinone **2** is resistant to acceptorless H_2 loss when heated in boiling toluene. Likewise, heating solid **2** to 200 °C under vacuum left the starting material unchanged.[46] These findings are in agreement with the calculated ΔG for the H_2 activation (Figure 4). When **2** was reacted with a large excess (at least 10 equiv) of diphenylacetylene as a hydrogen acceptor under UVB irradiation, the disappearance of **2** and formation of **1** were confirmed by IR spectroscopy. The concomitant formation of a 3:1 mixture of (*Z*) and (*E*)-stilbene was detected by GC−MS. The hydrogen transfer could also be observed with phenylacetylene as the substrate, yielding styrene and ethylbenzene in a 15:1 mixture as determined by GC−MS. Treating **1** with a dilute mineral acid like HCl yielded ferrahydroquinone chloride complex **4** (Scheme 5). As can be seen, the proton is transferred to the oxygen at the para position of the ligand while the chloride is bound to the metal center.

Organic quinones are known to undergo hydrogen−halogen exchange at the ring via halogen (X_2) addition followed by HX elimination.[12] We were interested to see whether similar behavior could be observed with ferraquinone **1**. Indeed, the reaction with 2.2 equiv of a 1 wt % solution of Br_2 in benzene

DOI: 10.1021/jacs.6b13050
J. Am. Chem. Soc. 2017, 139, 2799−2807

Scheme 5. Reaction of 1 with HCl via Formal 1,6-Addition

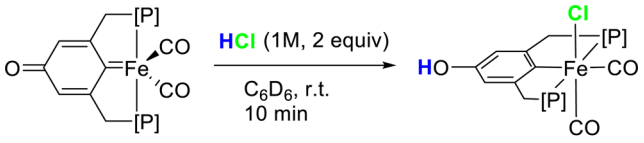

proceeded rapidly to form a new organometallic species. This compound was identified by NMR, FT-IR, MS, and X-ray crystallography to be ferrahydroquinone bromide **6** with the aryl moiety of the PCP pincer ligand brominated at both meta positions with respect to the metal (Scheme 6 and Figure 5).

Scheme 6. Formation of 5 by Treatment of 1 with Elemental Bromine

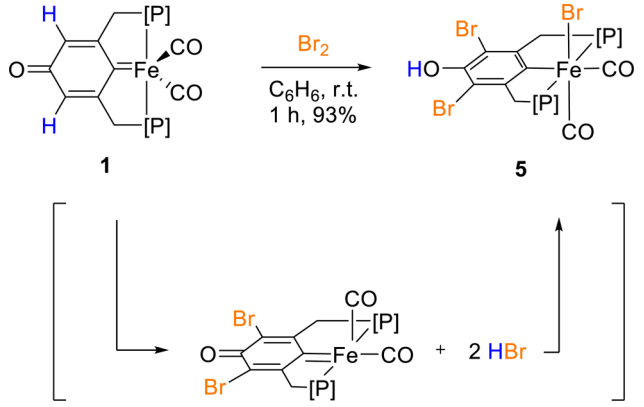

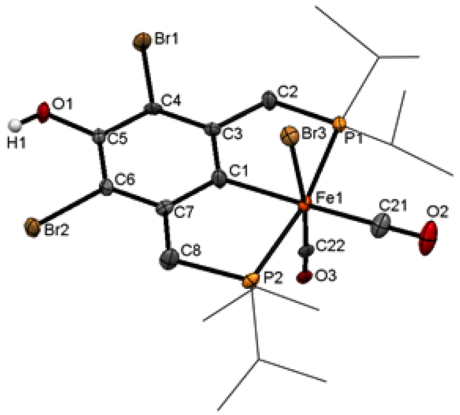

Figure 5. Solid-state structure of **5** (thermal ellipsoids set at the 50% probability level; isopropyl groups presented as wireframe and hydrogens omitted for clarity). Selected bond lengths [Å] and angles [deg] for **5**: Fe1–C21 1.813(4), Fe1–C22 1.765(4), Fe1–Br3 2.4900(7), Fe1–C1 2.031(4), Fe1–P1 2.268(1), Fe1–P2 2.279(1), C5–O1 1.356(4), C4–Br1 1.906(4), C6–Br2 1.904(3), C1–C3 1.404(5), C3–C4 1.392(5), C4–C5 1.396(5), P1–Fe1–P2 168.23(4), C1–Fe1–C21 177.3(2), C1–Fe1–Br3 89.1(1), C21–Fe1–C22 98.5.

The solid-state structure shows a slightly distorted octahedral geometry around the metal center with an Fe1–C1 bond length of 2.031(4) Å and an Fe1–Br3 distance of 2.4900(7) Å (Figure 5). In the ring moiety of the pincer ligand, the C–C bond lengths vary slightly between 1.392 and 1.405 Å and the C–O bond is a single bond at 1.356(4) Å, demonstrating aromaticity of the ring. The C–Br bond lengths are essentially equal (1.904(3) and 1.906(4) Å).

A likely mechanism for this transformation is analogous to hydrogen–halogen substitution in organic quinones, namely, Br_2 addition to the quinonic double bonds followed by HBr elimination. The HBr liberated during this step is immediately incorporated into the complex, akin to the reaction of **1** with HCl (Scheme 6).

Furthermore, it was found that upon standing in alcoholic solutions for 18 h at room temperature, ferraquinone **1** was also quantitatively converted into ferrahydroquinone **2**. The reaction time could be significantly decreased to 2 h by UVB irradiation. At the same time, formation of the corresponding aldehyde and no other organic products was observed by GC–MS. Short- and medium-chain aliphatic alcohols as well as benzyl alcohol were stochiometrically dehydrogenated to their corresponding aldehydes (Scheme 7).

Scheme 7. Dehydrogenation of Alcohols Mediated by 1

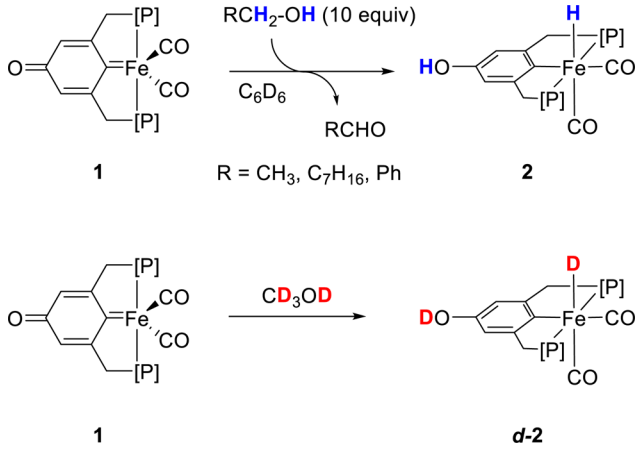

Using a deuterated alcohol like CD_3OD afforded *d*-**2** (Scheme 7), which was evident from the absence of a hydride signal in the ^1H NMR spectrum while the ^{31}P NMR spectrum displayed a 1:1:1 triplet at 110.5 ppm for the coordinated ligand, showing the coupling of the two equivalent phosphorus atoms with a deuteride. As in the reactions with H_2 and HCl, formal 1,6-type metal–ligand cooperation is involved in the oxidation of alcohols.

When a THF or benzene solution of **2** was exposed to air, an instantaneous color change to deep orange was observed. X-ray-quality crystals were obtained from a cooled toluene solution layered with diethyl ether, and the solid-state structure revealed the formation of oxyferraquinone **6**. One oxygen atom has been incorporated into the complex and bridges the metal center and the ipso carbon of the pincer ligand in a 1,2 fashion (Scheme 8).

Scheme 8. Formation of Oxaferraquinone 6 by Exposure of 2 to Oxygen

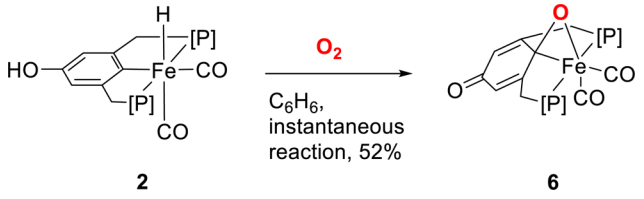

DOI: 10.1021/jacs.6b13050
J. Am. Chem. Soc. 2017, 139, 2799–2807

The solid-state bond lengths as well as computational analyses (natural bond orbital, Mayer bond order, and bond critical point analyses)[48] confirm that the best description of the bonding is that of a true metallaoxirane rather than a π-bonded carbonyl group, in contrast to our earlier observations with Ir-stabilized phenoxonium cations.[38] The character of the C(ipso)−O bond (C1−O4) is that of a single bond at 1.341(2) Å, while the C(para)−O bond (C5−O1) retains clear double-bond character with a bond length of 1.251(2) Å. The Fe1−C1 distance is 2.111(1) Å, only slightly longer than in complexes **2**, **4**, and **5**. The bond lengths in the ring alternate from a double bond for C3−C4 (1.359(2) Å) to single bonds for C1−C3 (1.458(2) Å) and C4−C5 (1.459(2) Å). The C1−O4 bond is 16.6° above and the C1−Fe1 bond 55.6° below the pincer ring plane, giving C1 the resemblance of a spiro junction of the six-membered and three-membered rings (Figure 6).

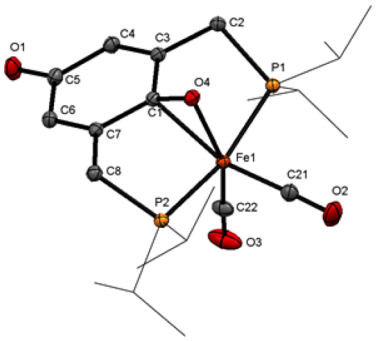

Figure 6. Solid-state structure of **6** (thermal ellipsoids set at the 50% probability level; isopropyl groups presented as wireframe and hydrogens omitted for clarity). Selected bond lengths [Å] and bond and torsion angles [deg] for **6**: Fe1−C21 1.780(1), Fe1−C22 1.764(1), Fe1−C1 2.111(1), Fe1−O4 1.9707(8), Fe1−P1 2.2633(4), Fe1−P2 2.2676(4), C1−O4 1.341(2), C5−O1 1.251(1), C1−C3 1.458(1), C3−C4 1.359(1), C4−C5 1.459 (2), P1−Fe1−P2 166.23(1), C1−Fe1−C21 147.80(5), Fe1−C1−O4 65.25(5), C3−C1−O4 119.39(9), C1−Fe1−O4 38.15(4), C1−O4−Fe1 76.60(5), C22−Fe1−C21 96.08(6), C1−Fe1−C22 116.11(5), C4−C3−C1−O4 163.4(1), C4−C3−C1−Fe1 124.4(1).

A recent report from our group describes the activation of dioxygen by metal−ligand cooperation involving the pincer side arms of a pyridine-based PNP−iridium complex.[47] Likewise, Goldberg[48,49] and more recently Piers[50] reported the formation of complexes in which an oxygen atom originating from O_2 or N_2O, respectively, bridges the metal center and the ligand in a fashion similar to that observed in **6**. However, we are not aware of a reported observed O_2 activation process involving O insertion into a metal−aryl bond.[51]

The mechanism of the activation of dioxygen by **2** was investigated by DFT calculations at the SMD(THF)-TPSS-D3BJ/def2-TZVPP//BP86-D3/def2-SV(P) level. Initial insertion of O_2 into the Fe−hydride bond via the long-range adduct $\mathbf{2.O_2}$ and $\mathbf{TS_{2.O2-7}}$ yields hydroperoxo complex **7** (Figure 7). A double-crossover pathway for this insertion can be found with a barrier of 19.7 kcal/mol, which would allow this step to occur at room temperature. Exergonic dimerization of **7** leads to the C_i-symmetric dimer **8**. Protonation of the hydroperoxy ligand by the hydroxyl group of the second molecule with concomitant C(ipso)−oxygen bond formation yields oxaferraquinone **6** and 1 equiv of water as a byproduct in an overall strongly exergonic reaction.

The experimental observation that a full equivalent of oxygen is necessary for the reaction to proceed to completion supports the proposed mechanism. Essential for the reaction is the formation of the interesting dimeric structure **8**. The DFT-optimized structure reveals intermolecular short hydrogen bonds between the *p*-hydroxyl group and the hydroperoxy ligand bound to the iron center of a second molecule (Figure 8). An analysis of the potential energy density at the bond critical point of these hydrogen bonds revealed that each single hydrogen bond stabilizes dimer **8** by −12.9 kcal/mol. These hydrogen bonds facilitate the protonation and weaken the O−O bond. Furthermore, the orientation of the hydroperoxy ligand in **8** allows for an interaction of the Fe−C(ipso) σ bond with the antibonding O−O σ^* bond of the hydroperoxy ligand, which is necessary for the S_N2-like C−O bond formation to occur (Figure 8).

In summary, we have developed a conceptually new metal−ligand cooperation pathway through an unprecedented ferraquinone−ferrahydroquinone couple. The metal center shows cooperativity with three different positions of the ligand in a formal 1,2 and 1,6 fashion depending on the reaction conditions, leading to a number of unique reactivity patterns. The ferraquinone reacts with alcohols to form aldehydes and lactones, thereby regenerating the ferrahydroquinone. In an unprecedented reaction for any metal complex, and analogous to reactions of organic quinones, it activates Br_2 and selectively incorporates it into the complex. The ferraquinone can be transformed to its hydrogenated form, the ferrahydroquinone, by activation of molecular hydrogen or alcohols. This compound instantaneously selectively activates molecular oxygen at room temperature by metal−ligand cooperation, resulting in O insertion into the aryl−Fe bond and formation of the corresponding oxyferraquinone. This novel mode of metal−ligand cooperation harnesses the reactivity of the metal center and the ligand at three different positions alike, and the described diversity in transformations and reactivity modes promises further fruitful studies with this motif.

EXPERIMENTAL DETAILS

General Specifications. All of the reactions were performed under a nitrogen atmosphere in a Vacuum Atmospheres Co. model Nexus glovebox or using standard Schlenk techniques, unless otherwise noted. All of the solvents were reagent grade or better. THF, diethyl ether, benzene, and pentane were refluxed over sodium, distilled under a nitrogen atmosphere, and stored over activated 3 Å molecular sieves. Dichloromethane was dried and stored over activated 3 Å molecular sieves. All of the commercially available reagents were used as received. UVB irradiation (280−315 nm) was performed in a Luzchem LZC-ORG photoreactor equipped with 10 lamps operated at 60 Hz (3 A, 220 V). The vessels used during irradiation were regular Pyrex glass Schlenk flasks. Experiments with quartz glass vessels yielded the same results and reaction times. NMR spectra were recorded using Bruker Avance III 300, Avance III 400, and Avance 500 spectrometers at 298 K. Chemical shifts were referenced to the residual solvent peaks (^{1}H, ^{13}C) or an external standard of phosphoric acid (85% solution in D_2O) at 0.0 ppm (^{31}P). Chemical shifts are reported in parts per million, and coupling constants (*J*) are reported in hertz. NMR assignments were assisted by ^{1}H−^{1}H COSY, ^{1}H−^{1}H NOESY, ^{1}H−^{13}C HSQC, and ^{1}H−^{13}C HMBC data. In the ^{13}C-DEPTQ NMR spectra, primary and tertiary carbon signals are phased down (d) and secondary and quaternary carbon signals are phased up (u). IR spectra were recorded on a Thermo Scientific Nicolet 6700 FT-IR spectrophotometer as thin films on NaCl or CaF_2 disks. Electrospray ionization mass spectrometry (ESI-MS) spectra were recorded on a Micromass ZQ V4.1 spectrometer by the Chemical

DOI: 10.1021/jacs.6b13050
J. Am. Chem. Soc. 2017, 139, 2799−2807

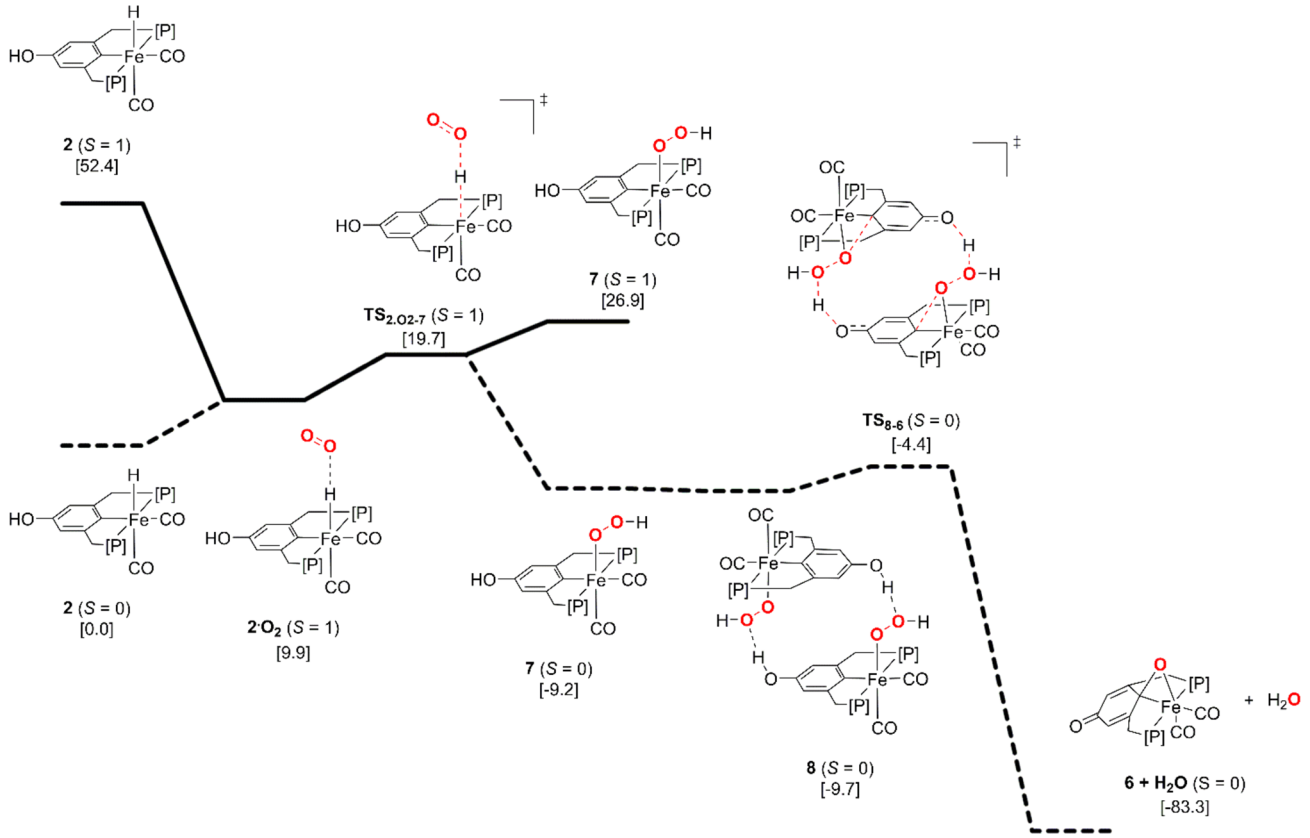

Figure 7. Free energy pathways for oxygen insertion into **2** calculated at the TPSS-D3BJ/def2-TZVPP//BP86-D3/def2-SV(P) level of theory. Solvent effects were implicitly taken into account using the SMD model. All of the free energies are given with respect to **2** and $^3O_2$ (and **7** in the case of **8** and $\mathbf{TS}_{8-6}$).

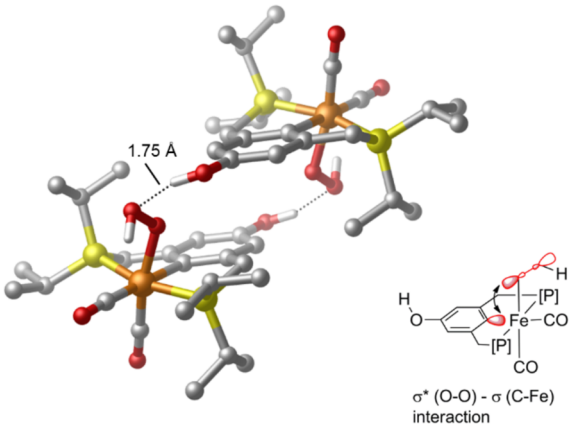

Figure 8. DFT-optimized structure of **8** with a schematic representation of the interaction of the Fe−C(ipso) σ bond with the O−O σ^* bond. The computed O···HO hydrogen bond length is shown.

Research Support Unit of the Weizmann Institute of Science. Crystal data for complexes **4**, **5**, and **6** were measured at 100 K on a Bruker Kappa Apex-II CCD diffractometer equipped with Mo Kα radiation (λ = 0.710 73 Å), a graphite monochromator, and MiraCol optics. The data were processed with APEX2 collect package programs. Structures were solved by the AUTOSTRUCTURE module and refined with full-matrix least-squares refinement based on F^2 with SHELXL-2013.

Data for complex **2** were collected on APEX2 and then in the synchrotron ESRF ID-29. Data were processed with HKL2000, keeping the Friedel pairs (FPs) separate. The structure was solved with SHELXT. The best suggested solution was the noncentrosymmetric space group *Pc* with 12 molecules in the asymmetric unit cell and a Flack parameter of 0.49, and most of the isopropyl side chains were missing. The data were processed again with CrysAlisPro, keeping the FPs separate, and the initial solution with SHELXT contained almost all of the atoms (including the isopropyl side chains). The structure was further refined with SHELXL-2013 with full-matrix least-squares refinement based on F^2. The refinement was extremely complex because of the high levels of molecular disorder and twinning. Many constraints were applied in order to bring the refinement to completion. The hydride was calculated and placed at 1.5 Å from the metal center in direct extension of the Fe−CO bond.

Synthesis of 1. *Method A.* In a 5 mL vial equipped with a Teflon stir bar was placed **2** (10 mg, 0.021 mmol) in dry benzene (1 mL), and the solution was stirred. A solution of benzoquinone (4.5 mg, 0.042 mmol) was added, and the reaction mixture turned from yellow to deep orange-brown. The mixture was stirred for 30 min at room temperature and then filtered, and the solvent was removed in vacuo. The crude residue was extracted with pentane (5 × 0.5 mL), and the extracts were combined and dried to give a dark-orange powder (8 mg, 0.018 mmol, 86%). *Method B.* In a 20 mL scintillation vial equipped with a Teflon stir bar was placed **4** (150 mg, 0.300 mmol) in dry benzene (6 mL) and the solution was stirred. A solution of KHMDS (72 mg, 0.360 mmol) was added dropwise, and the reaction mixture turned from yellow to deep orange-brown with some precipitate formation. The mixture was stirred for 30 min at room temperature and then filtered, and the solvent was removed in vacuo. The crude material was extracted with pentane (5 × 3 mL), and the extracts were pooled and dried to give a dark-orange powder (83 mg, 0.179 mmol, 60%). ^{1}H NMR (300 MHz, C_6D_6) δ ppm 6.87 (s, 2H, *Ar*), 3.77−3.10 (m, 4H, Ar−CH_2−P), 2.44 (br s, 2H, $CH_{(iPr)}$), 2.07 (br s, 2H, $CH_{(iPr)}$), 1.61−0.62 (m, 24H, *iPr*). ^{13}C{^{1}H} NMR (126 MHz, C_6D_6) δ ppm 217.8(u) (t, J_{C-P} = 27.5 Hz, *CO*), 214.8(u) (t, J_{C-P} = 11.8 Hz, *CO*), 170.1(u) (s, C═*O*), 148.4(u) (s, *Ar*), 117.1(d) (br s, *Ar*), 37.2.4(u)

DOI: 10.1021/jacs.6b13050
J. Am. Chem. Soc. 2017, 139, 2799−2807

(br s, Ar−CH_2−P), 26.5(d) (t, J_{C-P} = 7.6 Hz, $CH_{(iPr)}$), 25.2(d) (t, J_{C-P} = 25.1 Hz, $CH_{(iPr)}$), 19.9(d) (s, *iPr*), 19.8(d) (s, *iPr*), 19.5(d) (s, *iPr*), 19.4(d) (s, *iPr*). $^{31}P\{^1H\}$ NMR (121 MHz, C_6D_6) δ ppm 94.5. IR 1983, 1921, 1563 cm^{-1}. HRMS (ESI) calcd 465.1411 ($C_{22}H_{34}O_3P_2Fe$ + H^+), found 465.1409.

Synthesis of 2. In a 100 mL Schlenk flask equipped with a Teflon stir bar was placed **3** (400 mg, 1.13 mmol) in dry THF (15 mL). $Fe(CO)_5$ (200 mg, 1.02 mmol) was added, and the flask was sealed and put in a UVB reactor with stirring at room temperature. CO gas forming in the course of the reaction was vented after 6 h and again after 18 and 48 h. After 4 days, the reaction mixture was emerald green, and the volatiles were removed in vacuo. The residue was washed with pentane (3 × 5 mL) and dried to yield **2** as a green powder (390 mg, 0.837 mmol, 82%). Crystals (fine needles) suitable for X-ray analysis were obtained by slow diffusion of pentane into a solution of **2** in Et_2O/pentane (1:1). ^1H NMR (300 MHz, C_6D_6) δ ppm 6.48 (s, 2H, *Ar*), 3.86 (br s, 1H, Ar*OH*), 3.15−2.93 (m, 2H, Ar−CH_2−P), 2.79 (dt, *J* = 16.48, 4.58 Hz, 2H, Ar−CH_2−P), 2.10−1.74 (m, 4H, $CH_{(iPr)}$) 1.32−0.98 (m, 18H, *iPr*), 0.92−0.76 (m, 6H, *iPr*) −8.81 (t, J_{H-P} = 50.4 Hz, 1H, Fe−H). $^{13}C\{^1H\}$ NMR, DEPT-Q (126 MHz, C_6D_6) δ ppm 217.2(u) (t, *J* = 15.5 Hz, *CO*), 216.5(u) (t, *J* = 12.0 Hz, *CO*), 159.3(u) (t, J_{C-P} = 13.4 Hz, *Ar*C−Fe), 153.6(u) (s, *Ar*C−OH), 147.1(u) (t, J_{C-P} = 10.2 Hz, *Ar*), 109.9(d) (s, *Ar*), 39.4(u) (t, J_{C-P} = 13.6 Hz, Ar−CH_2−P), 28.4(d) (t, J_{C-P} = 9.2 Hz, $CH_{(iPr)}$), 26.9(d) (t, J_{C-P} = 14.3 Hz, $CH_{(iPr)}$), 18.9(d) (s, *iPr*), 18.7(d) (s, *iPr*), 18.5(d) (s, *iPr*), 18.1(d) (s, *iPr*). $^{31}P\{^1H\}$ NMR (121 MHz, C_6D_6) δ ppm 111.5 (s). IR 1967, 1920, 1888 (Fe−H), 1590 cm^{-1}. Anal. Calcd for $C_{22}H_{36}FeO_3P_2$: C, 56.67; H, 7.78; Fe, 11.98; O, 10.29; P, 13.28. Found: C, 56.46; H, 8.26.

Synthesis of 3. Bis(bromomethyl)phenol was prepared according to a literature procedure.[14] In a thick-walled 250 mL round-bottom flask equipped with a Teflon stir bar was placed a solution of the dibromide (2.82 g, 10 mmol) and diisopropylphosphine (5.88 g, 50 mmol) in methanol (30 mL). The flask was sealed with a Teflon screw cap, and the clear, amber solution was heated to 50 °C with stirring for 2 days. Triethylamine (8.3 mL, 60 mmol) was added under an inert atmosphere, and the resulting solution was stirred for 30 min at room temperature. The volatiles were removed in vacuo, after which the residue was taken up repeatedly in diethyl ether and the volatiles were removed again in vacuo (4 × 20 mL). The ligand was crystallized from a cooled and highly concentrated pentane solution to give colorless crystals (2.93 g, 8.26 mmol, 83%). ^1H NMR (300 MHz, C_6D_6) δ ppm 6.96 (s, 1H, *Ar*), 6.67 (s, 2H, *Ar*), 4.80 (br s, 1H, Ar*OH*), 2.63 (s, 4H, Ar−CH_2−P), 1.60 (h, 4H, $CH_{(iPr)}$), 0.99 (m, 24H, *iPr*). $^{31}P\{^1H\}$ NMR (121 MHz, C_6D_6) δ ppm 9.5 (s).

Synthesis of 4. In a 20 mL scintillation vial equipped with a Teflon stir bar was placed **2** (100 mg, 0.215 mmol) in dry benzene (5 mL). The vial was sealed with a septum screw cap, and the mixture was stirred. Concentrated aqueous HCl (50 μL, 0.54 mmol) was added dropwise, and the reaction mixture turned from green to yellow with some gas evolution. The mixture was stirred for 1 h at room temperature, and the volatiles were removed in vacuo. The crude material was extracted with THF (3 × 2 mL), and the filtered extracts were combined and dried to give **4** as a light-yellow powder (93 mg, 0.186 mmol, 87%). ^1H NMR (400 MHz, $CDCl_3$) δ ppm 6.63 (s, 2 H, *Ar*), 4.47 (br s, 1 H, Ar*OH*), 3.57 (dt, *J* = 15.6, 4.6 Hz, 2H, Ar−CH_2−P), 3.33 (dt, *J* = 15.6, 3.7 Hz, 2H, Ar−CH_2−P), 3.03−2.89 (m, 2H, $CH_{(iPr)}$), 2.51−2.35 (m, 2H, $CH_{(iPr)}$), 1.45−1.32 (m, 12H, *iPr*), 1.30−1.20 (m, 12H, *iPr*). $^{13}C\{^1H\}$ NMR, DEPT-Q (100.7 MHz, $CDCl_3$) δ ppm 216.1(u) (t, J_{C-P} = 25.6 Hz, *CO*), 212.1(u) (t, J_{C-P} = 13.6 Hz, *CO*), 160.0(u) (t, J_{C-P} = 12.8 Hz, *Ar*C−Fe), 154.2(u) (s, *Ar*C−OH), 148.3(u) (t, J_{C-P} = 8.5 Hz, *Ar*) 110.9(d) (t, J_{C-P} = 7.4 Hz, *Ar*), 37.7(u) (t, J_{C-P} = 15.0 Hz, Ar−CH_2−P), 26.1(d) (t, J_{C-P} = 9.9 Hz, $CH_{(iPr)}$) 24.9 (t, J_{C-P} = 9.9 Hz, $CH_{(iPr)}$), 19.7(d) (s, *iPr*), 19.6(d) (s, *iPr*), 19.5(d) (s, *iPr*), 19.3(d) (s, *iPr*). $^{31}P\{^1H\}$ NMR (162.1 MHz, $CDCl_3$) δ ppm 94.1 (s). IR 1995, 1932 cm^{-1}.

Synthesis of 5. In a 20 mL scintillation vial equipped with a Teflon stir bar was placed **1** (20 mg, 0.043 mmol) in dry benzene (3 mL). The vial was sealed with a septum screw cap, and the mixture was stirred. A solution of Br_2 in dry benzene (1 wt %, 0.5 mL, 0.097 mmol) was added dropwise, and the reaction mixture turned from dark brown-orange to a vibrant bright orange. The mixture was stirred for 1 h at room temperature and filtered, and the volatiles were removed in vacuo. The crude material was extracted with pentane/Et_2O (1:1, 3 × 2 mL), and the filtered extracts were combined and dried to give **5** as a bright-orange powder (28 mg, 0.040 mmol, 93%). Crystals (prisms) suitable for X-ray analysis were obtained by slow diffusion of pentane into a solution of **5** in Et_2O/pentane (1:1). ^1H NMR (400 MHz, C_6D_6) δ ppm 5.60 (br s, 1H, Ph*OH*), 3.89 (dt, *J* = 16.5, 4.3 Hz, 2H, Ar−CH_2−P), 3.48 (dt, *J* = 16.5, 3.6 Hz, 2H, Ar−CH_2−P), 3.12−2.99 (m, 2H, $CH_{(iPr)}$), 2.02−1.89 (m, 2H, $CH_{(iPr)}$), 1.22−1.09 (m, 6H, *iPr*), 1.07−0.85 (m, 18H, *iPr*). ^{13}C NMR, DEPT-Q (100.7 MHz, C_6D_6) δ ppm 217.5(u) (t, J_{C-P} = 25.7 Hz, *CO*), 212.7(u) (t, J_{C-P} = 14.5 Hz, *CO*), 160.5(u) (t, J_{C-P} = 13.6, *Ar*C−Fe), 147.1(u) (s, *Ar*C−OH), 146.2(u) (t, J_{C-P} = 8.2 Hz, *Ar*) 107.4(u) (t, J_{C-P} = 7.0 Hz, *Ar*), 40.8(u) (t, J_{C-P} = 15.8 Hz, Ar−CH_2−P), 26.5(d) (t, J_{C-P} = 10.7 Hz, $CH_{(iPr)}$), 26.4(d) (t, J_{C-P} = 9.8 Hz, $CH_{(iPr)}$), 19.4(d) (s, *iPr*), 19.3(d) (s, *iPr*), 19.1(d) (s, *iPr*), 19.0(d) (s, *iPr*). ^{31}P NMR (162.1 MHz, C_6D_6) δ ppm 84.7 (s). IR 2003, 1941 cm^{-1}. LRMS (ESI) 724.89 (highest-abundance peak, 1:3:3:1 isotope pattern for three Br) ($C_{22}H_{33}Br_3O_3P_2Fe$ + Na^+).

Synthesis of 6. In a 20 mL scintillation vial equipped with a Teflon stir bar was placed **2** (60 mg, 0.129 mmol) in dry benzene (5 mL). The vial was removed from the glovebox, and a stream of O_2 was bubbled through the solution for 10 s. The dark mixture was filtered, yielding a black filter residue and a bright orange filtrate. The volatiles of the filtrate were removed in vacuo to give **6** as a bright-orange powder (32 mg, 0.067 mmol, 52%). Crystals (prisms) suitable for X-ray analysis were obtained by slow diffusion of pentane into a solution of **6** in toluene.

To test the stoichiometry of the reaction, the reaction was repeated under identical conditions with the addition of only 0.5 equiv or 1 equiv of O_2 via a gastight syringe through a septum. The workup was performed in an analogous fashion inside the glovebox, and it was found that in the case of the addition of only 0.5 equiv of O_2 that the conversion of the starting material was not complete. In contrast, in the case of addition of a full 1 equiv of O_2, the starting material was fully consumed. ^1H NMR (400 MHz, C_6D_6) δ ppm 6.53 (s, 2H, *Ar*), 2.58−2.38 (m, 2H, Ar−CH_2−P), 1.89−1.73 (m, 2H, $CH_{(iPr)}$), 1.72−1.53 (m, 2H, $CH_{(iPr)}$), 1.44−1.24 (m, 6H, *iPr*), 1.19−0.75 (m, 14H, Ar−CH_2−P and *iPr*), 0.74−0.59 (m, 6 H, *iPr*) (residual toluene at 2.1 ppm). $^{13}C\{^1H\}$ NMR, DEPT-Q (100.7 MHz, C_6D_6) δ ppm 217.0(u) (t, *J* = 21.1 Hz, *CO*), 215.60(u) (t, *J* = 22.7 Hz, *CO*) 183.6(u) (s, Ar*C*═*O*), 157.4(u) (s, *Ar*), 124.6(d) (t, *J* = 5.1 Hz, *Ar*), 96.7(u) (t, *J* = 2.2 Hz, *Ar*C−Fe), 26.4(d) (t, *J* = 10.2 Hz, $CH_{(iPr)}$), 20.2(u) (t, *J* = 9.6 Hz, Ar−CH_2−P), 17.9(d) (s, *iPr*), 17.4(d) (s, *iPr*), 17.0(d) (s, *iPr*), 16.7(d) (s, *iPr*). $^{31}P\{^1H\}$ NMR (162.1 MHz, C_6D_6) δ ppm 69.4 (s). IR 1967, 1904 cm^{-1}. LRMS (ESI) 503.19 ($C_{22}H_{34}O_4P_2Fe$ + Na^+). Anal. Calcd for $C_{22}H_{34}FeO_4P_2$: C, 55.02; H, 7.14; Fe, 11.63; O, 13.32; P, 12.90. Found: C, 54.47; H, 7.62.

Computational Details. All of the geometries were optimized with the BP86 generalized-gradient approximation (GGA) functional and the def2-SV(P) basis set together with the corresponding core potential for iron. The D3 dispersion correction was used for the geometry optimizations. Thermodynamic properties were obtained at the same level of theory from frequency calculations. All of the free energies were calculated under standard conditions, unless otherwise noted. Minima and transition states were characterized by the absence and presence of one imaginary frequency, respectively. For comparison with the experimentally observed IR spectra, the structures of **1**, **2**, **4**, and **6** were reoptimized at the same level of theory with the larger def2-TZVP basis set. Single-point calculations were obtained with the TPSS meta-GGA functional in combination with the D3 dispersion correction, Becke−Johnson dumping, and the larger triple-ζ plus polarization def2-TZVPP basis set. The TPSS functional was recently shown to yield results very close to explicitly correlated coupled-cluster benchmark calculations for reaction energies and barriers involving transition metal complexes with pincer ligands. In order to improve the computational efficiency, the density fitting approximation with the W06 fitting basis sets, designed for use with the def2 basis sets, was used. In order to take solvent effects into account, the SMD solvation

DOI: 10.1021/jacs.6b13050
J. Am. Chem. Soc. 2017, 139, 2799−2807

model for THF was used for the single-point calculations. The "ultrafine" grid (i.e., a pruned (99,590) grid) was used for all of the calculations. All of the calculations were performed using Gaussian 09, revision D.01.

■ ASSOCIATED CONTENT

Supporting Information

The Supporting Information is available free of charge on the ACS Publications website at DOI: 10.1021/jacs.6b13050.

Experimental details of synthetic procedures, X-ray data, and computational details (PDF)

Crystallographic data for **2**, **4**, **5**, and **6** (CIF)

■ AUTHOR INFORMATION

Corresponding Author

*david.milstein@weizmann.ac.il

ORCID

David Milstein: 0000-0002-2320-0262

Author Contributions

§A.D. and U.G. contributed equally.

Notes

The authors declare no competing financial interest.

■ ACKNOWLEDGMENTS

This research was supported by the European Research Council (ERC AdG 692775) and by the Kimmel Center for Molecular Design. A.D. thanks the Austrian Science Fund for an Erwin Schrödinger Postdoctoral Fellowship and the Azrieli Foundation for a Research and Materials Grant. U.G. thanks the DAAD for a Postdoctoral Fellowship and the Feinberg Graduate School for a Senior Postdoctoral Award. D.M. holds the Israel Matz Professorial Chair of Organic Chemistry. We thank Linda J. W. Shimon for collecting data at ERSF ID-29, and the staff members of ERSF ID-29 are acknowledged for their support.

■ REFERENCES

(1) *The Chemistry of the Quinoid Compounds, Parts 1 and 2*; Patai, S., Ed.; Wiley: London, 1974. *The Chemistry of the Quinoid Compounds, Parts 1 and 2*; Patai, S., Rappoport, Z., Eds.; Wiley: Chichester, U.K., 1988.

(2) Campos-Martin, J. M.; Blanco-Brieva, G.; Fierro, J. L. G. *Angew. Chem., Int. Ed.* **2006**, *45*, 6962−6984.

(3) Abraham, I.; Joshi, R.; Pardasani, P.; Pardasani, R. *J. Braz. Chem. Soc.* **2011**, *22*, 385−421.

(4) Bäckvall, J.-E.; Hopkins, R. B.; Grennberg, H.; Mader, M.; Awasthi, A. K. *J. Am. Chem. Soc.* **1990**, *112*, 5160−5166. Piera, J.; Bäckvall, J.-E. *Angew. Chem., Int. Ed.* **2008**, *47*, 3506−3523.

(5) Zhang, Y.; Li, C.-J. *J. Am. Chem. Soc.* **2006**, *128*, 4242−4243.

(6) Guo, X.; Zipse, H.; Mayr, H. *J. Am. Chem. Soc.* **2014**, *136*, 13863−13873.

(7) Lerch, S.; Unkel, L.-N.; Brasholz, M. *Angew. Chem., Int. Ed.* **2014**, *53* (25), 6558−6562.

(8) Lerch, S.; Unkel, L.-N.; Wienefeld, P.; Brasholz, M. *Synlett* **2014**, *25*, 2673−2680.

(9) Zhou, L.; Xu, B.; Zhang, J. *Angew. Chem., Int. Ed.* **2015**, *54*, 9092−9096.

(10) Ernster, L.; Dallner, G. *Biochim. Biophys. Acta, Mol. Basis Dis.* **1995**, *1271*, 195−204.

(11) Ernster, L.; Forsmark-Andrée, P. *Clin. Invest.* **1993**, *71* (Suppl. 8), S60−S65.

(12) Milton, R. D.; Hickey, D. P.; Abdellaoui, S.; Lim, K.; Wu, F.; Tan, B.; Minteer, S. D. *Chem. Sci.* **2015**, *6*, 4867−4875.

(13) Bauer, I.; Knölker, H.-J. *Chem. Rev.* **2015**, *115*, 3170−3387.

(14) Bolm, C.; Legros, J.; Le Paih, J.; Zani, L. *Chem. Rev.* **2004**, *104*, 6217−6254.

(15) Enthaler, S.; Junge, K.; Beller, M. *Angew. Chem., Int. Ed.* **2008**, *47*, 3317−3321.

(16) Langer, R.; Leitus, G.; Ben-David, Y.; Milstein, D. *Angew. Chem., Int. Ed.* **2011**, *50*, 2120−2124.

(17) Langer, R.; Diskin-Posner, Y.; Leitus, G.; Shimon, L. J. W.; Ben-David, Y.; Milstein, D. *Angew. Chem., Int. Ed.* **2011**, *50*, 9948−9952.

(18) Langer, R.; Iron, M. A.; Konstantinovski, L.; Diskin-Posner, Y.; Leitus, G.; Ben-David, Y.; Milstein, D. *Chem. - Eur. J.* **2012**, *18*, 7196−7209.

(19) Zell, T.; Butschke, B.; Ben-David, Y.; Milstein, D. *Chem. - Eur. J.* **2013**, *19*, 8068−8072.

(20) Srimani, D.; Diskin-Posner, Y.; Ben-David, Y.; Milstein, D. *Angew. Chem., Int. Ed.* **2013**, *52*, 14131−14134.

(21) Rivada-Wheelaghan, O.; Dauth, A.; Leitus, G.; Diskin-Posner, Y.; Milstein, D. *Inorg. Chem.* **2015**, *54* (9), 4526−4538.

(22) Butschke, B.; Fillman, K. L.; Bendikov, T.; Shimon, L. J. W.; Diskin-Posner, Y.; Leitus, G.; Gorelsky, S. I.; Neidig, M. L.; Milstein, D. *Inorg. Chem.* **2015**, *54*, 4909−4926.

(23) Zell, T.; Milstein, D. *Acc. Chem. Res.* **2015**, *48* (7), 1979−1994.

(24) Garg, J. A.; Chakraborty, S.; Ben-David, Y.; Milstein, D. *Chem. Commun.* **2016**, *52*, 5285−5288.

(25) Rivada-Wheelaghan, O.; Chakraborty, S.; Shimon, L. J. W.; Ben-David, Y.; Milstein, D. *Angew. Chem., Int. Ed.* **2016**, *55*, 6942−6945.

(26) Ashkenazi, N.; Vigalok, A.; Parthiban, S.; Ben-David, Y.; Shimon, L. J. W.; Martin, J. M. L.; Milstein, D. *J. Am. Chem. Soc.* **2000**, *122*, 8797−8798.

(27) Vigalok, A.; Rybtchinski, B.; Gozin, Y.; Koblenz, T. S.; Ben-David, Y.; Rozenberg, H.; Milstein, D. *J. Am. Chem. Soc.* **2003**, *125*, 15692−15693.

(28) Vigalok, A.; Milstein, D. *Acc. Chem. Res.* **2001**, *34*, 798−807.

(29) (a) Vigalok, A.; Milstein, D. *J. Am. Chem. Soc.* **1997**, *119*, 7873−7874. (b) Poverenov, E.; Milstein, D. Quinone Methide Stabilization by Metal Complexation. In *Quinone Methides*; Rokita, S. E., Ed.; Wiley: Hoboken, NJ, 2009; pp 69−88.

(30) Kharisov, B.; Méndez-Rojas, M.; Garnovskii, A.; Ivakhnenko, E.; Ortiz-Méndez, U. *J. Coord. Chem.* **2002**, *55*, 745−770.

(31) Kim, S. B.; Pike, R. D.; Sweigart, D. A. *Acc. Chem. Res.* **2013**, *46*, 2485−2497.

(32) (a) Moussa, J.; Amouri, H. *Angew. Chem., Int. Ed.* **2008**, *47*, 1372−1380. (b) Moussa, J.; Lev, D. A.; Boubekeur, K.; Rager, M. N.; Amouri, H. *Angew. Chem., Int. Ed.* **2006**, *45*, 3854−3858. (c) Amouri, H.; Moussa, J.; Renfrew, A. K.; Dyson, P. J.; Rager, M. N.; Chamoreau, L.-M. *Angew. Chem., Int. Ed.* **2010**, *49*, 7530−7533. (d) Amouri, H.; Le Bras, J. *Acc. Chem. Res.* **2002**, *35*, 501−510. (e) Moussa, J.; Guyard-Duhayon, C.; Herson, P.; Amouri, H.; Rager, M. N.; Jutand, A. *Organometallics* **2004**, *23*, 6231−6238.

(33) Mitsumi, M.; Ezaki, K.; Komatsu, Y.; Toriumi, K.; Miyatou, T.; Mizuno, M.; Azuma, N.; Miyazaki, Y.; Nakano, M.; Kitagawa, Y.; Hanashima, T.; Kiyanagi, R.; Ohhara, T.; Nakasuji, K. *Chem. - Eur. J.* **2015**, *21*, 9682−9696.

(34) Zhang, S.-S.; Jiang, C.-Y.; Wu, J.-Q.; Liu, X.-G.; Li, Q.; Huang, Z.-S.; Li, D.; Wang, H. *Chem. Commun.* **2015**, *51*, 10240−10243.

(35) Horak, K. T.; Agapie, T. *J. Am. Chem. Soc.* **2016**, *138*, 3443−3452.

(36) Review: Khusnutdinova, J. R.; Milstein, D. *Angew. Chem., Int. Ed.* **2015**, *54*, 12236−12273.

(37) Grützmacher, H. *Angew. Chem., Int. Ed.* **2008**, *47*, 1814−1818.

(38) van der Vlugt, J. I. *Eur. J. Inorg. Chem.* **2012**, *2012*, 363−375.

(39) Ikariya, T. *Top. Organomet. Chem.* **2011**, *37*, 31−53.

(40) Gunanathan, C.; Milstein, D. *Acc. Chem. Res.* **2011**, *44*, 588−602.

(41) Becauses of the extreme air sensitivity of the crystals, the resulting data were often insufficient for full refinement. It was found serendipitously that exposing the crystals to air for an extended period of time resulted in better diffraction data. This was attributed to the likely formation of a protective but nondiffracting oxide layer on the surface of the crystal.

DOI: 10.1021/jacs.6b13050
J. Am. Chem. Soc. 2017, 139, 2799−2807

(42) Bhattacharya, P.; Krause, J. A.; Guan, H. *Organometallics* **2011**, *30*, 4720−4729.
(43) de Sanctis, D.; Beteva, A.; Caserotto, H.; Dobias, F.; Gabadinho, J.; Giraud, T.; Gobbo, A.; Guijarro, M.; Lentini, M.; Lavault, B.; Mairs, T.; Mcsweeney, S.; Petitdemange, S.; Rey-Bakaikoa, V.; Surr, J.; Theveneau, P.; Leonard, G. A.; Mueller-Dieckmann, C. *J. Synchrotron Radiat.* **2012**, *19*, 455−461.
(44) Complexes in which a metal-coordinated carbene cannot be detected by ^{13}C NMR spectroscopy have been reported. See: (a) Alcarazo, M.; Roseblade, S. J.; Cowley, A. R.; Fernández, R.; Brown, J. M.; Lassaletta, J. M. *J. Am. Chem. Soc.* **2005**, *127*, 3290−3291. (b) Mayr, M.; Wurst, K.; Ongania, K.-H.; Buchmeiser, M. R. *Chem. - Eur. J.* **2004**, *10* (5), 1256−1266. (c) Coleman, K. S.; Chamberlayne, H. T.; Turberville, S.; Green, M. L. H.; Cowley, A. R. *Dalton Trans.* **2003**, *14*, 2917−2922.
(45) For full computational details and calculations, see the Supporting Information.
(46) When the compound was heated to a melt under vacuum, a complex product mixture was formed that according to FT-IR spectroscopy contained **1** but was NMR-silent and eluded further characterization.
(47) Feller, M.; Ben-Ari, E.; Diskin-Posner, Y.; Carmieli, R.; Weiner, L.; Milstein, D. *J. Am. Chem. Soc.* **2015**, *137*, 4634−4637.
(48) Scheuermann, M. L.; Fekl, U.; Kaminsky, W.; Goldberg, K. I. *Organometallics* **2010**, *29*, 4749−4751.
(49) Scheuermann, M. L.; Luedtke, A. T.; Hanson, S. K.; Fekl, U.; Kaminsky, W.; Goldberg, K. I. *Organometallics* **2013**, *32*, 4752−4758.
(50) Doyle, L. E.; Piers, W. E.; Borau-Garcia, J. *J. Am. Chem. Soc.* **2015**, *137*, 2187−2190.
(51) Zhang, Y.-H.; Yu, J.-Q. *J. Am. Chem. Soc.* **2009**, *131*, 14654−14655.

DOI: 10.1021/jacs.6b13050
J. Am. Chem. Soc. 2017, 139, 2799−2807